HHS Public Access

Towards real-time topical detection and characterization of FDG dose infiltration prior to PET imaging

Jason M. Williams[1,*], **Lori R. Arlinghaus**[1], **Sudheer D. Rani**[1,2], **Martha D. Shone**[2], **Vandana G. Abramson**[3,4], **Praveen Pendyala**[5], **A. Bapsi Chakravarthy**[4,5], **William J. Gorge**[6], **Joshua G. Knowland**[6], **Ronald K. Lattanze**[6], **Steven R. Perrin**[6], **Charles W. Scarantino**[6,7], **David W. Townsend**[6,8], **Richard G. Abramson**[1,2,4], and **Thomas E. Yankeelov**[9]

[1]Vanderbilt University Institute of Imaging Science, Vanderbilt University Medical Center, Nashville, Tennessee, USA

[2]Department of Radiology and Radiological Sciences, Vanderbilt University Medical Center, Nashville, Tennessee, USA

[3]Department of Medicine, Vanderbilt University Medical Center, Nashville, Tennessee, USA

[4]Vanderbilt-Ingram Cancer Center, Nashville, Tennessee, USA

[5]Department of Radiation Oncology, Vanderbilt University Medical Center, Nashville, Tennessee, USA

[6]Lucerno Dynamics, LLC, Morrisville, North Carolina, USA

[7]Department of Radiation Oncology, University of North Carolina, Chapel Hill, North Carolina, USA

[8]Clinical Imaging Research Centre, Agency for Science, Technology and Research-National University of Singapore, Singapore, Singapore

[9]Institute for Computational and Engineering Sciences, and Departments of Biomedical Engineering and Internal Medicine, The University of Texas at Austin, Austin, Texas, USA

Abstract

*Correspondence: Jason M. Williams, Ph.D., 1161 21st Avenue South, AA-1105 Medical Center North, Nashville, TN 37232-2310, Phone: (615) 343-7753, Fax: (615) 322-0734, jason.m.williams@vanderbilt.edu.

Purpose—To dynamically detect and characterize ^{18}F-fluorodeoxyglucose (FDG) dose infiltrations and evaluate their effects on positron emission tomography (PET) standardized uptake values (SUV) at the injection site and in control tissue.

Methods—Investigational gamma scintillation sensors were topically applied to patients with locally advanced breast cancer scheduled to undergo limited whole-body FDG-PET as part of an ongoing clinical study. Relative to the affected breast, sensors were placed on the contralateral injection arm and ipsilateral control arm during the resting uptake phase prior to each patient's PET scan. Time activity curves (TACs) from the sensors were integrated at varying intervals (0–10, 0–20, 0–30, 0–40, and 30–40 min) post-FDG and the resulting areas-under-the-curve (AUCs) were compared to SUVs obtained from PET.

Results—In cases of infiltration, observed in three sensor recordings (30%), the injection arm TAC shape varied depending on the extent and severity of infiltration. In two of these cases TAC characteristics suggested the infiltration was partially resolving prior to image acquisition, although it was still apparent on subsequent PET. Areas under the TAC 0–10 and 0–20 min post-FDG were significantly different in infiltrated versus non-infiltrated cases (Mann-Whitney, $p <$ 0.05). When normalized to control, all TAC integration intervals from the injection arm were significantly correlated with SUV_{peak} and SUV_{max} measured over the infiltration site (Spearman ρ 0.77, $p < 0.05$). Receiver operating characteristic (ROC) analyses, testing the ability of the first 10 minutes of post-FDG sensor data to predict infiltration visibility on the ensuing PET, yielded an area under the ROC curve of 0.92.

Conclusion—Topical sensors applied near the injection site provide dynamic information from the time of FDG administration through the uptake period and may be useful in detecting infiltrations regardless of PET image field of view. This dynamic information may also complement the static PET image to better characterize the true extent of infiltrations.

Introduction

^{18}F-Fluorodeoxyglucose (FDG) PET/CT plays a pivotal role in cancer care. A widely used parameter to quantify FDG uptake is the standardized uptake value (SUV), calculated by normalizing FDG activity concentration in a volume of interest (VOI) to the decay-corrected injected activity and body mass. SUVs allow semi-quantitative evaluation of disease and therapy response. Accuracy of SUV estimation assumes the entire net injected dose is administered intravenously as a bolus injection. Improper injections can result in 21–50% change in SUV measurements [1, 2]. A recent summary of findings from six prospective, randomized controlled studies evaluating peripheral IV catheter infiltration rates found a mean incidence of 23.9% [3]. In the few published studies measuring infiltration rates in PET, tracer infiltration occurs in 10–21% of clinical exams [2, 4, 5].

Dose infiltrations are particularly concerning in oncology where venous integrity is often compromised due to disease and/or therapy. Moreover, the antecubital vein—the most

common FDG injection site—is often excluded from the commonly-used PET base-of-skull to mid-thigh field of view (FOV), as standard body imaging is performed with arms raised to avoid artefacts in CT-based attenuation correction [6]. Infiltrations may thus go undetected and unreported, as demonstrated in a recent study where 31% of those detected occurred outside the base-of-skull to mid-thigh FOV [4], and documentation of the injection site location relative to the FOV was missing in at least 8% of oncologic PET reports [7].

Failing to account for, report, or even detect dose infiltrations confounds SUV measurements by overestimating injected tracer activity [1] and by underestimating the time that FDG is available for tissue uptake, which severely hinders the quantitative use of PET. We tested the hypothesis that an investigational gamma radiation detection system [8] applied to the skin near the FDG injection site could dynamically detect and characterize the occurrence of infiltrations during the uptake phase preceding whole-body PET/CT.

Materials and methods

Patients

Eight women with locally advanced breast carcinoma participating in a clinical trial (ClinicalTrials.gov NCT01222416) examining FDG-PET/CT for early prediction of neoadjuvant therapy response [9] consented to this study, which was approved by the Institutional Review Board. Two patients had a follow-up FDG-PET/CT as part of the parent trial, resulting in a total of 10 datasets.

Sensor application and FDG-PET/CT

PET/CT was performed according to standard protocols [6]. After confirming fasting blood glucose (median 92.5 mg/dl, range 83 – 117, $n = 10$) and gaining venous access (antecubital vein, $n = 9$; metacarpal vein, $n = 1$), investigational scintillation sensors [8] (Lucerno Dynamics, LLC, Morrisville, NC, USA; Fig. 1) were attached topically with medical tape in three locations: over the tumour, 10 cm above the antecubital fossa contralateral to the tumour (injection arm), and 10 cm above the ipsilateral antecubital fossa (control arm). The unshielded sensors contain a Bismuth Germanate crystal with corresponding photodetector, resulting in an iso-sensitivity profile that is approximately spherical, with a centre located at the centre of the detector face. Activity recording from the sensors was initiated approximately 60 s prior to injection of FDG (median 453 MBq, range 359 – 522, $n = 10$) followed by a 10–20 ml saline flush. Administration of FDG was performed by five Certified Nuclear Medicine Technologists having a median of 13 (range 5 – 20) years of experience. Patients remained inactive in a dimmed room while sensor data were recorded during the resting uptake period. Sensors operated in 2-second cycles: 1 second to count the activity followed by 1 second to record the data. Near the end of the uptake period (42 – 59 min post-FDG) sensors were removed, and patients underwent limited whole-body PET/CT (i.e., top-of-skull to mid-thigh FOV) in a Discovery STE scanner (GE Healthcare, Waukesha, WI, USA) as previously described [10].

Data analysis

Areas under the time activity curve (TAC), in units of integrated counts, were computed over various intervals, including the initial bolus FDG infusion (median 0.8 min post-injection; range 0.3 – 1.9 min), as well as fixed time intervals of 0–10, 0–20, 0–30, 0–40, and 30–40 min post-injection. For these intervals, the ratio of the injection arm TAC area to the control arm TAC area was computed, and referred to as the *I/C ratio* (i.e., injection to control ratio). The median (± 95% confidence interval) I/C ratio for the last 10 min of sensor recordings, the portion of the TAC closest in time to PET, was computed; the upper confidence limit served as a threshold for detection. PET data were converted to SUVs on a voxel-wise basis according to standard methods [11]. VOIs were drawn over the antecubital fossa and right hepatic lobe (background) to compute the maximum single-voxel SUV in the VOI (SUV_{max}) and the mean value of a 1 cm^3 sphere placed in the most FDG-avid portion of the VOI (SUV_{peak}), which also included SUV_{max} [12]. Data underwent nonparametric group comparisons in Prism (GraphPad, La Jolla, CA, USA); correlation analyses, and receiver operating characteristic (ROC) analyses in Matlab (Mathworks, Natick, MA, USA). For ROC analyses, the visibility of an infiltration on the PET image served as the 'gold standard'. Maximum intensity projections (MIPs) were generated in OsiriX (OsiriX Foundation, Geneva, Switzerland).

Results

In ten sensor-PET data pairs, FDG infiltration was detected in three TACs (30%). A fourth scan featured a FDG spot at the site of injection. This spot was low in intensity and volume and was not detected by the sensor but was observable on PET only. Sensor data were collected for a median of 51.6 min (range 42.1 – 60.0). The median duration from FDG injection to start of PET was 73.1 min (range 60.0 – 80.9).

Fig. 2 depicts TACs obtained from sensor recordings in five illustrative cases. Supplemental Figure 1 includes sensor data TACs from the injection and control arms for all 10 cases. The injection arm TAC (red trace, *top*) was normalized point-by-point to the control arm TAC (blue trace, *top*) to determine the injection/control (I/C) ratio (purple trace, *bottom*). In the six scans where no infiltration was visible on PET, the median (± 95% confidence interval) I/C ratio for the last 10 min of sensor recordings was 1.14 (± 0.21). The upper confidence limit (I/C ratio = 1.35) denotes a convenient reference threshold for infiltration detection (black dotted line).

The patient shown in Case 1 had no detectable evidence of infiltration based on the injection arm and control arm sensor TACs (Fig. 2a). This patient experienced a steep rise and fall and large amplitude of the injection arm TAC during the first 45 s post-FDG administration and was consistent with the kinetics of an unimpeded intravenous bolus (Fig. 2a). In sharp contrast, the patient shown in Case 2 experienced severe, persistent dose infiltration at the injection site, as suggested by the shallow slope of the injection arm TAC and approximately 19-fold greater area under the TAC relative to the control arm (Fig. 2b). Case 3 had moderate dose infiltration that resolved to a small infiltration during the uptake period and approximately 2-fold greater area under the TAC relative to control (Fig. 2c). The patient in Case 4 initially exhibited a severe infiltration that resolved to a moderate infiltration prior to

the PET scan and approximately 9-fold greater area under the TAC relative to control (Fig. 2d). In Case 5, a small spot of FDG near the site of injection was evident on PET (see below), but, because the injection arm sensor was placed 10 cm proximal, the spot was not detected and the TAC shape appeared normal (Fig. 2e).

Fig. 3 shows maximum intensity projections (MIPs), obtained from PET acquisitions that followed the sensor data acquisitions, for each of the five illustrative cases in Fig. 2. Case 1 had no visible evidence of infiltration on PET (Fig. 3a); the median ($\pm$ 95%CI) injection site-to-background (liver) SUV_{peak} ratio for the six non-infiltrated scans was 0.38 ($\pm$ 0.069). Conversely, Case 2 exhibited severe infiltration in the antecubital fossa, with 674-fold higher SUV_{peak} in the injection arm versus liver (Fig. 3b). Case 3, where the sensor data suggested the infiltration had resolved to a low level, had residual FDG uptake in the antecubital fossa that was 3.3-fold higher relative to liver (Fig. 3c). For Case 4, where the sensor data indicated a severe infiltration that resolved to a moderate infiltration by the end of the uptake period, moderate FDG infiltration was visible in the antecubital fossa, which had a SUV_{peak} at least nine times higher than liver (Fig. 3d). As mentioned above, a small FDG spot was visible in the injection site for Case 5, with an SUV_{peak} approximately 1.5 times higher than liver (Fig. 3e).

Supplemental Table 1 summarizes the various sensor TAC integration metrics obtained from the injection and control arm sensors, as well as SUV_{max} and SUV_{peak} measurements obtained from antecubital fossa of the injection arm and right liver lobe background for all 10 PET scans. Fig. 4 summarizes results of nonparametric statistical comparisons (Mann-Whitney test) of sensor and PET data obtained in PET-visible infiltration ($n = 4$) versus non-infiltration ($n = 6$) groups. Following the initial FDG infusion peak, significant differences ($p < 0.05$) between infiltrated and non-infiltrated groups were apparent for the 0–10 min and 0–20 min sensor TAC integration metrics as well as the PET SUV metrics (Fig. 4). Table 1 summarizes the nonparametric (Spearman) correlation analyses of sensor TAC integration and PET SUV measurements, which collectively show that, by normalizing the injection arm data to control data, the correlation is improved; all sensor TAC integration I/C ratios were significantly correlated with antecubital fossa SUV_{peak} and SUV_{max} normalized to liver (Spearman ρ 0.77, $p < 0.05$). Receiver operating characteristic (ROC) analyses, summarized in Table 2, were conducted to determine the diagnostic capabilities of the sensors to predict whether an infiltration would be visible on the subsequent PET image. Data collected over the first 10 and 20 minutes post-FDG were most predictive, resulting in an area under the ROC curve of 0.92.

Discussion

This is the first report demonstrating the feasibility of topically applied scintillation sensors for detecting and characterizing FDG dose infiltrations in real time. We showed five examples where the shape of the sensor TAC yielded dynamic information regarding the amount of FDG counts recorded approximately 10 cm from the injection site (Fig. 2). Statistically significant differences ($p < 0.05$) between infiltrated and non-infiltrated TACs were observed in the first 20 min following FDG injection (Fig. 4). Additionally, TAC integration metrics 0–40 min post-FDG were significantly correlated ($p < 0.05$) with PET

SUVs when the parameters were normalized to their respective background, e.g., injection arm/control arm for TAC integrations and antecubital fossa/liver VOIs for PET SUVs (Table 1). Furthermore, ROC analyses indicated that information obtained from the sensors, even within the first 10 min following the initial administration of FDG, had a high degree of accuracy for predicting the appearance of infiltration in the subsequent PET scan (Table 2). Given the frequency of infiltrations, which have ranged from 10–24% [2–5], these findings highlight the value of sensitive methods capable of quantitatively reporting on the fidelity of intravenous radiotracer injection *before* image acquisition as an important quality control procedure to verify the clinical reliability of the SUVs obtained from the PET scan.

Quantitative PET requires rigorous standardization of image acquisition and analysis [1, 12, 13]. Underscoring this point, a recent multicentre study of non-small cell lung cancer found a 30% SUV decrease (in defining therapeutic response) or a 40% SUV increase (in defining progression) is required to have confidence that the results are indicative of metabolic response or metabolic progression, rather than a reflection of the variability in the PET/CT measurement process [14]. It is likely that infiltration of FDG at the injection site would contribute to this variability [1, 2]. An infiltration reduces the delivered dose and reduces the available uptake time in ways that cannot be accurately accounted for using information in a static PET image. The results from the current study suggest that lower metabolic response thresholds for PET may be achievable if the variability introduced by infiltrations is reduced. Indeed, considering the range of temporal manifestations (e.g., persisting or resolving throughout the uptake period, Fig. 2b–d), the occurrence of an infiltration would likely completely invalidate the use of SUVs in the study, since they cannot be accurately corrected *post hoc*.

While clinical impressions for staging disease based upon PET are generally qualitative, quantitative data are essential in therapy response evaluation and would undoubtedly also improve disease staging [12]. Topical scintillation sensors may provide immediate feedback regarding the onset and severity of an infiltration in ways that could be critically useful in PET. Identifying severe infiltrations at the end of the uptake period is not a challenge *if* the injection site is in the FOV; the PET image shows the infiltration, confirmed by the sensor data. Perhaps the more useful aspect is identification of cases where the infiltration was severe for an appreciable part of the uptake period, but resolves towards the end. In these cases, even if the injection site is in the PET FOV, PET data would understate the extent of the infiltration, but dynamic sensor data from the uptake period would identify it clearly. For this reason, sensor data could provide a valuable and currently unavailable characterization of an infiltration.

Providing feedback on the fidelity of an FDG injection could help reduce erroneous interpretations and provide options, not available currently, for clinicians in the management of their patients. In non-quantitative studies, awareness of a resolving infiltration before PET acquisition may provide clinicians the opportunity to prolong the uptake period. Having visibility to severe infiltrations that resolve dramatically prior to PET imaging provides clinicians information that may lead to repeating critically important scans.

The preliminary findings presented here have certain inherent limitations. One is that the study includes only a small number of matched observations ($n = 10$) and, perhaps owing to this, a potentially higher infiltration rate (30% confirmed by both sensors and PET) than might be expected. This is in contrast to the infiltration rate seen in studies with larger patient cohorts (11–21% confirmed by PET alone) [2, 4, 5]. A further limitation of this study is related to the placement of the sensor with respect to the injection site. In a follow-on, multicentre clinical assessment of approximately 400 patients since the evaluation of the device at Vanderbilt began, infiltration rates of ~22% have been confirmed (unpublished data). In this same study, placement of the sensors approximately 7 cm from the injection site has provided improved sensitivity allowing for the detection of residual FDG in indwelling catheters. A similar approach of surface detection at locations proximal to the venous access site has also been demonstrated with technetium-99m probes [15].

In the future, additional studies will provide insight regarding other important possibilities that arise from this work. Due to the unshielded nature of the detectors, the use of sensor ratios (i.e., injection arm/control arm) to establish detection thresholds for predicting infiltration visibility on PET could be influenced by physiologic and/or pathologic uptake of FDG into nearby organs, an effect which needs further investigation. Additionally, studies assessing the impact of infiltrations on quantification using reference regions, dynamic TAC sensor data, and quantitative dynamic modelling could provide additional insight as to the consequences of infiltration. Finally, a third possible use of the sensors that would be of particular interest for dynamic PET studies would be to provide an estimate of the arterial input function without the need for invasive blood sampling.

In conclusion, it is evident that failing to account for FDG dose infiltration would lead to quantitative errors in SUV estimates and would also influence qualitative interpretations of PET scans. Since a static PET image is incapable of characterizing the quality of FDG administration during the preceding ~60 min uptake period, topical scintillation sensors could provide a simple as well as economical approach for real-time feedback on the occurrence and extent of dose infiltration.

Supplementary Material

Refer to Web version on PubMed Central for supplementary material.

Acknowledgments

References

1. Boellaard R. Standards for PET image acquisition and quantitative data analysis. J Nucl Med. 2009; 50(Suppl 1):11S–20S. DOI: 10.2967/jnumed.108.057182 [PubMed: 19380405]

2. Hall NC, Zhang J, Reid R, Hurley D, Knopp MV. Impact of FDG extravasation on SUV measurements in clinical PET/CT. Should we routinely scan the injection site? J Nucl Med. 2006; 47(Supplement 1):115P.

3. Helm RE, Klausner JD, Klemperer JD, Flint LM, Huang E. Accepted but unacceptable: peripheral IV catheter failure. J Infus Nurs. 2015; 38(3):189–203. DOI: 10.1097/NAN.0000000000000100 [PubMed: 25871866]

4. Osman MM, Muzaffar R, Altinyay ME, Teymouri C. FDG dose extravasations in PET/CT: frequency and impact on SUV measurements. Front Oncol. 2011; 1:41.doi: 10.3389/fonc. 2011.00041 [PubMed: 22655246]

5. Silva-Rodriguez J, Aguiar P, Sanchez M, Mosquera J, Luna-Vega V, Cortes J, et al. Correction for FDG PET dose extravasations: Monte Carlo validation and quantitative evaluation of patient studies. Med Phys. 2014; 41(5):052502.doi: 10.1118/1.4870979 [PubMed: 24784399]

6. Delbeke D, Coleman RE, Guiberteau MJ, Brown ML, Royal HD, Siegel BA, et al. Procedure guideline for tumor imaging with 18F-FDG PET/CT 1.0. J Nucl Med. 2006; 47(5):885–95. doi: 47/5/885 [pii]. [PubMed: 16644760]

7. Coleman RE, Hillner BE, Shields AF, Duan F, Merlino DA, Hanna LG, et al. PET and PET/CT reports: observations from the National Oncologic PET Registry. J Nucl Med. 2010; 51(1):158–63. DOI: 10.2967/jnumed.109.066399 [PubMed: 20008997]

8. Knowland, JG.; Scarantino, CW.; Lattanze, RK. System for the detection of gamma radiation from a radioactive analyte. Google Patents. US 20130324844 A1. 2013.

9. Atuegwu NC, Li X, Arlinghaus LR, Abramson RG, Williams JM, Chakravarthy AB, et al. Longitudinal, intermodality registration of quantitative breast PET and MRI data acquired before and during neoadjuvant chemotherapy: preliminary results. Med Phys. 2014; 41(5):052302.doi: 10.1118/1.4870966 [PubMed: 24784395]

10. Williams JM, Rani SD, Li X, Arlinghaus LR, Lee TC, MacDonald LR, et al. Comparison of prone versus supine 18F-FDG-PET of locally advanced breast cancer: Phantom and preliminary clinical studies. Med Phys. 2015; 42(7):3801.doi: 10.1118/1.4921363 [PubMed: 26133582]

11. QIBA FDG-PET/CT Standardized Uptake Value (SUV) Technical Subcommittee. Vendor-neutral pseudo-code for SUV calculation. QIBA/RSNA. http://qibawiki.rsna.org/index.php?title=Standardized_Uptake_Value_(SUV). Accessed August 30, 2015

12. Wahl RL, Jacene H, Kasamon Y, Lodge MA. From RECIST to PERCIST: Evolving considerations for PET response criteria in solid tumors. J Nucl Med. 2009; 50(Suppl 1):122S–50S. doi:50/Suppl_1/122S[pii]10.2967/jnumed.108.057307. [PubMed: 19403881]

13. Kinahan PE, Mankoff DA, Linden HM. The value of establishing the quantitative accuracy of PET/CT imaging. J Nucl Med. 2015; 56(8):1133–4. DOI: 10.2967/jnumed.115.159178 [PubMed: 26089552]

14. Weber WA, Gatsonis CA, Mozley PD, Hanna LG, Shields AF, Aberle DR, et al. Repeatability of 18F-FDG PET/CT in advanced non-small cell lung cancer: prospective assessment in 2 multicenter trials. J Nucl Med. 2015; 56(8):1137–43. DOI: 10.2967/jnumed.114.147728 [PubMed: 25908829]

15. Bonta DV, Halkar RK, Alazraki N. Extravasation of a therapeutic dose of 131I-metaiodobenzylguanidine: prevention, dosimetry, and mitigation. J Nucl Med. 2011; 52(9):1418–22. DOI: 10.2967/jnumed.110.083725 [PubMed: 21795365]

Fig. 1.
(a) Sensors containing scintillation material convert gamma radiation, emitted from the decay of ^{18}F-FDG, to visible light in the form of photon counts/sec. For recordings of the injection arm and control arm, sensors are positioned over the bicep, since the convex shape of the antecubital fossa hinders direct recording from this region. Sensors are held in place using standard medical tape. **(b)** Sensors are connected via cable to a portable reader module that actively records activity counts at 1-second intervals. Data from each sensor channel (up to four) are digitized, tabulated and exported from the reader in a variety of formats for further computational analysis.
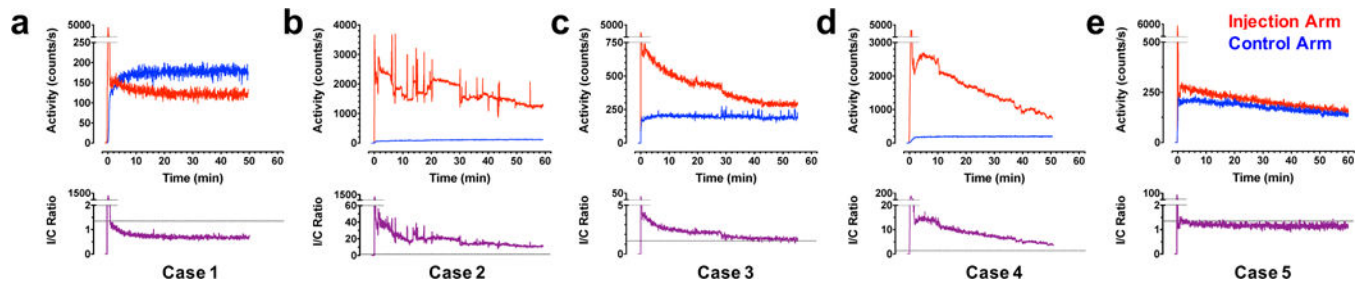
Fig. 2.

Time activity curves (TACs) from sensors placed over the injection arm (red) were normalized to those obtained on the control arm (blue) to determine the I/C ratio (purple) in a patient with no visible infiltration (**a**) and patients with severe (**b**), moderate that resolves to small (**c**), and severe that resolves to moderate (**d**) infiltration. PET data corresponding to each of these cases are found in Fig. 3. One patient (**e**) had a low activity spot of FDG, visible on PET (Fig. 3e), but TAC data were inconclusive due to sensor distance from this spot. Note the differential ordinate scaling; see Supplemental Figure 1 for TAC data from all 10 scans.
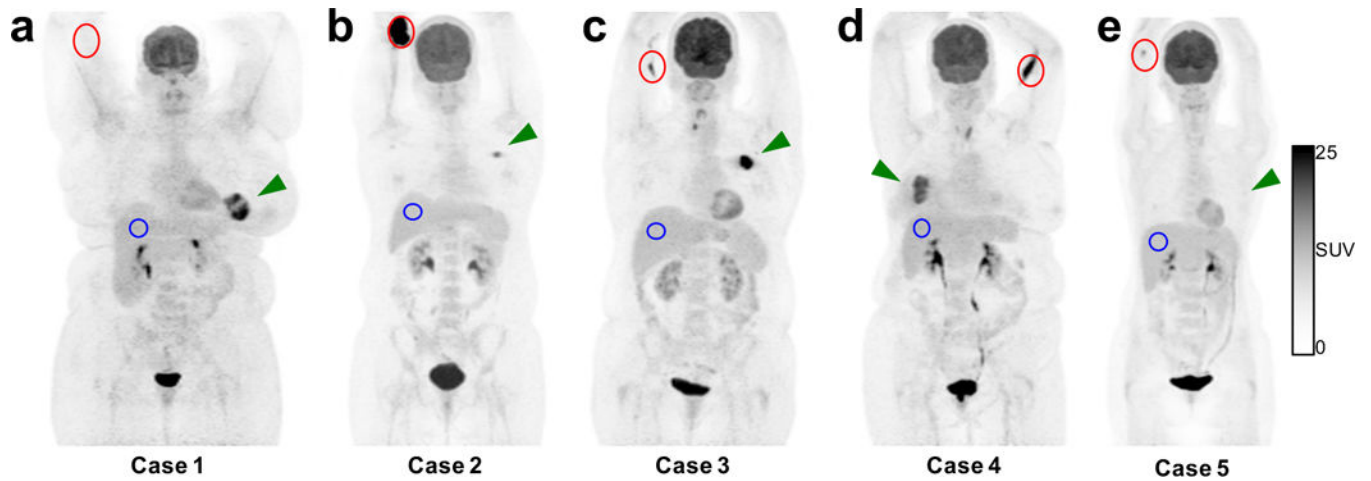
Fig. 3.
Maximum intensity projections from PET images, corresponding to the sensor time activity curves (TACs) in Fig. 2, illustrate the antecubital injection site (red), hepatic control site (blue), and tumour (green arrow) in a patient with no visible infiltration (**a**) and patients with severe (**b**), small (**c**), and moderate (**d**) infiltration. One patient (**e**) had a low activity spot of FDG that was not detected by the sensor, but TAC data (Fig. 2e) were inconclusive due to sensor distance to this spot.
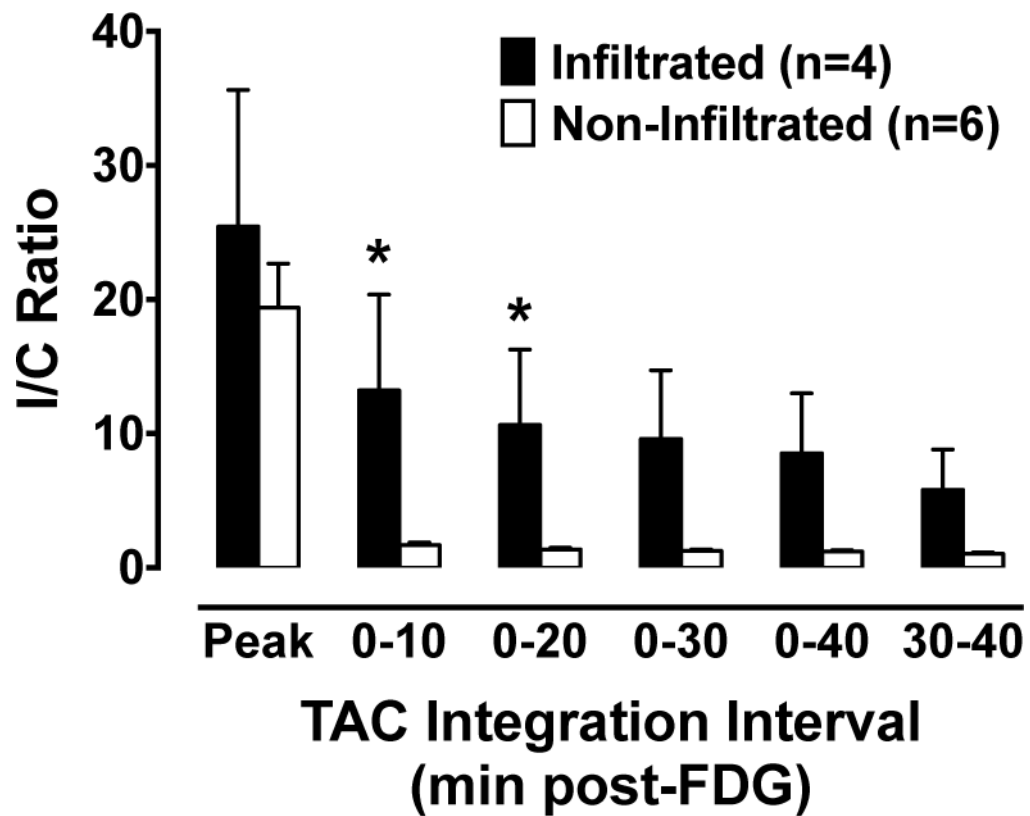
Fig. 4.
Injection arm (I) sensor TAC areas were normalized to control arm (C) sensor TAC areas to compute the I/C Ratio over a range of intervals during the uptake period (Peak only; 0–10; 0–20; 0–30; 0–40; and 30–40 post-FDG). Significant differences between infiltrated (dark bars) and non-infiltrated (open bars) were observed in the 0–10 and 0–20 min post-FDG intervals (p<0.05 Mann-Whitney test).

Table 1

Correlation of sensor and PET metrics. Sensor data (TAC areas, integrated counts) determined over various intervals are well correlated with SUV data from subsequent PET.

TAC interval	Sensor arm	Sensor metric vs. SUVmax		Sensor metric vs. SUVpeak	
		ρ^a	p	ρ^a	p
Peak only	Injection	0.503	0.143	0.479	0.166
Peak only	I/C ratio	0.297	0.407	0.297	0.407
0–10 min	Injection	0.673	0.039	0.758	0.016
0–10 min	I/C ratio	0.806	0.008	0.806	0.008
0–20 min	Injection	0.612	0.067	0.709	0.028
0–20 min	I/C ratio	0.903	0.001	0.903	0.001
0–30 min	Injection	0.564	0.096	0.673	0.039
0–30 min	I/C ratio	0.903	0.001	0.903	0.001
0–40 min	Injection	0.515	0.133	0.612	0.067
0–40 min	I/C ratio	0.842	0.005	0.842	0.005
30–40 min	Injection	0.382	0.279	0.467	0.178
30–40 min	I/C ratio	0.770	0.014	0.770	0.014

TAC, time activity curve; *AUC*, area-under-curve; *I/C*, injection/control (contralateral arm for sensors; right liver lobe for PET); *SUV*, standardized uptake value.

[a] Spearman rank correlation coefficient.

Table 2

Receiver operating characteristic analyses of sensor diagnostic performance. Ability of integration metrics from the sensor TACs to predict whether an infiltration will be visible on ensuing PET: infiltration visible ($n = 4$); infiltration not visible ($n = 6$).

TAC interval	Sensor arm	ROC area	Sensitivity	Specificity	Cut-off value	PPV	NPV
Peak only	Injection	0.71	50%	100%	1.76×10^5	100%	75.0%
Peak only	I/C ratio	0.58	50%	100%	29.20	100%	75.0%
0–10 min	Injection	0.92	75%	100%	3.34×10^5	100%	85.7%
0–10 min	I/C ratio	0.92	75%	100%	2.62	100%	85.7%
0–20 min	Injection	0.92	75%	100%	5.40×10^5	100%	85.7%
0–20 min	I/C ratio	0.92	75%	100%	1.87	100%	85.7%
0–30 min	Injection	0.88	75%	100%	7.48×10^5	100%	85.7%
0–30 min	I/C ratio	0.88	75%	100%	1.61	100%	85.7%
0–40 min	Injection	0.83	75%	100%	9.45×10^5	100%	85.7%
0–40 min	I/C ratio	0.83	75%	100%	1.47	100%	85.7%
30–40 min	Injection	0.79	75%	100%	1.97×10^5	100%	85.7%
30–40 min	I/C ratio	0.88	75%	100%	1.31	100%	85.7%

TAC, time activity curve; *ROC*, receiver operating characteristic; *I/C*, injection arm/control arm; *PPV*, positive predictive value; *NPV*, negative predictive value.